Mon. Not. R. Astron. Soc. **000**, 000–000 (0000) Printed 30 October 2015 (MN LATEX style file v2.2)

Oscillations of radiation pressure supported tori near black holes

Grzegorz P. Mazur[1,2⋆], Olindo Zanotti[3]†, Aleksander Sądowski[4,5]‡,
Bhupendra Mishra[2],Wlodek Kluźniak[2]

[1] *Institute of Physics, Polish Academy of Sciences, al. Lotników 32/46, 02-668 Warsaw, Poland*
[2] *Nicolaus Copernicus Astronomical Center, Bartycka 18, 00-716 Warsaw, Poland*
[3] *Laboratory of Applied Mathematics, University of Trento, Via Mesiano 77, 38123 Trento, Italy*
[4] *MIT Kavli Institute for Astrophysics and Space Research, 77 Massachusetts Ave, Cambridge, MA 02139, USA*
[5] *Einstein Fellow*

arXiv:1510.08810v1 [astro-ph.HE] 29 Oct 2015

30 October 2015

ABSTRACT

We study the dynamics of radiation pressure supported tori around Schwarzschild black holes, focusing on their oscillatory response to an external perturbation. Using KORAL, a general relativistic radiation hydrodynamics code capable of modeling all radiative regimes from the optically thick to the optically thin, we monitor a sample of models at different initial temperatures and opacities, evolving them in two spatial dimensions for ~ 165 orbital periods. The dynamics of models with high opacity is very similar to that of purely hydrodynamics models, and it is characterized by regular oscillations which are visible also in the light curves. As the opacity is decreased, the tori quickly and violently migrate towards the gas-pressure dominated regime, collapsing towards the equatorial plane. When the spectra of the L_2 norm of the mass density are considered, high frequency inertial-acoustic modes of oscillations are detected (with the fundamental mode at a frequency $68 M_{\rm BH}^{-1}$ Hz), in close analogy to the phenomenology of purely hydrodynamic models. An additional mode of oscillation, at a frequency $129 M_{\rm BH}^{-1}$ Hz, is also found, which can be unambiguously attributed to the radiation. The spectra extracted from the light curves are typically more noisy, indicating that in a real observation such modes would not be easily detected.

Key words: accretion, accretion discs – black hole physics – methods: numerical

1 INTRODUCTION

Starting from the seminal papers by Shakura & Sunyaev (1973) and Novikov & Thorne (1973), the physics of accretion discs around black holes has been extensively studied, both on a theoretical ground and by means of numerical simulations (see, e.g., Abramowicz & Fragile 2013, and references therein). In the last two decades numerical studies related to accretion discs have allowed to obtain a good understanding of complex phenomena such as the development of hydrodynamical and magnetohydrodynamical instabilities, the generation and propagation of jets in magnetically dominated regions, the actual role of the Blandford & Znajek mechanism, the dynamics of tilted discs, and so on. In spite of these progresses, most of the relativistic numerical investigations carried out so far have neglected the role of the radiation field. The situation is now rapidly changing, and in the last years quite a few time-dependent numerical radiative codes have been developed and applied to various physical systems related to accretion flows in a relativistic context (Farris et al. 2008; Zanotti et al. 2011; Fragile et al. 2012; Roedig et al. 2012; McKinney et al. 2013; Sądowski et al. 2013; Takahashi & Ohsuga 2013; Sądowski et al. 2014).

One of the phenomena that has been attracting a lot of attention among theoreticians is represented by the periodic response of geometrically thick discs to perturbations. These objects were introduced almost 40 years ago as stationary and axisymmetric solutions of a fluid in non-Keplerian circular motion around a black hole (Fishbone & Moncrief 1976; Abramowicz et al. 1978; Kozlowski et al. 1978). Although they can be regarded as toy models under many respects, they are still considered as a realistic approximation of the inner part of a much larger accretion disc. Their astrophysical relevance was further revitalized once it was found that they can exhibit a regular oscillating behaviour when subject to generic external perturbations (Zanotti et al. 2003; Zanotti et al. 2005; Blaes et al. 2006). In fact, the dynamics of geometrically thick discs was thereafter studied in connection to the phenomenology of the high frequency quasi-periodic oscillations (kHz-QPOs) observed in the X-ray spectra of binary systems (Remillard & McClintock 2006), for which they could provide more than one plausible interpretation [see, among the others, Rezzolla et al. (2003); Abramowicz et al. (2003); Schnittman & Rezzolla (2006); Blaes et al. (2007); Montero & Zanotti (2012); Mazur et al. (2013); Vincent et al. (2014); Bakala et al. (2015)]. In this context, Mishra

⋆ E-mail: gmazur@ifpan.edu.pl (GM)
† E-mail: olindo.zanotti@unitn.it (OZ)
‡ E-mail: asadowsk@mit.edu (AS)

© 0000 RAS

et al. (2015) have recently studied the response of a hydrodynamical torus to various perturbations and used sophisticated ray-tracing to obtain luminosity curves assuming both large and small optical depth.

In this paper we wish to perform a step forward along this direction of research by studying the role of the radiation field on the very oscillations of radiation pressure-dominated tori. To this extent, we resort to the radiative general relativistic code KORAL (Sądowski et al. 2013, 2014), which incorporates a number of very desirable features, such as i) the conservative formulation of the equations, ii) the implicit treatment of radiative source terms and iii) the ability in capturing both the optically thick and the optically thin regimes, by means of a suitable relativistic version of the M1-closure scheme. After considering the long-term evolution of a few but representative models in two spatial dimensions, we find that the dynamics of the tori is strongly dependent on the opacity and produces light curves which contain the in-printing of the perturbation. Although in our analysis we do not take into account important radiation processes like bremsstrahlung or synchrotron, our results testify the importance of a proper physical and numerical modelling of radiation processes in a relativistic context. We emphasize that we do not aim at proposing any specific new model for the kHz-QPOs phenomenology, but rather we extend the numerical study of oscillating tori to optically thick, radiation-pressure supported objects.

In the following, we adopt a geometrized system of units by setting $c = G = 1$, although we resort to cgs units when convenient. In particular, we adopt $r_{\rm g} = GM/c^2$ and $t_{\rm g} = GM/c^3$ as units of distance and time, respectively.

2 NUMERICAL SETUP

2.1 Initial configuration

Constant angular momentum tori, which are stationary and axisymmetric solutions of the relativistic hydrodynamics equations for a perfect fluid can be built following Kozlowski et al. (1978) [see also Font & Daigne (2002)]. The resulting hydrodynamic model provides the distribution of the total pressure, $p_{\rm tot}$, of the rest-mass density ρ, as well as of the orbital velocity Ω, which is super-Keplerian in the inner part of the torus up to the radius of maximum density, while it is sub-Keplerian in the outer part. The gas obeys the ideal gas equation of state $p = \rho\epsilon(\Gamma - 1)$, where Γ is the adiabatic index and ϵ is the specific (i.e. per unit mass) internal energy.

We decided to simulate the oscillations of a class of relativistic tori described by constant specific angular momentum $\ell = -u_\phi/u_t = 3.8$ with the inner and outer edges at $r_{\rm in} = 6.54$ and $r_{\rm out} = 11.0$, respectively. The jump of the effective potential W between $r_{\rm in}$ and the position of the cusp is $W_{\rm in} - W_{\rm cusp} = -7.37\times10^{-3}$, meaning that the equilibrium configuration remains below the marginally stable one [see Font & Daigne (2002) for more details]. The density of the torus is adjusted through the entropy parameter, which also affects the Thomson scattering opacity. Specific values are given in Table 1.

When radiation is also considered, we assume that initially $\Gamma = 4/3$, consistently with the assumption of a radiation pressure dominated disc. The total pressure obtained in this way is then distributed between the gas and the radiation, in such a way to satisfy local thermal equilibrium (LTE), i.e. $\widehat{E} = 4\sigma T^4$. This involves solving the following quartic equation for gas (and radiation) temperature (Sądowski et al. 2014)

$$p_{\rm tot} = p_{\rm gas} + p_{\rm rad} = k_{\rm B}\rho T + \frac{4}{3}\sigma T^4\,, \qquad (1)$$

where $k_{\rm B}$ and σ are the Boltzmann and the Stefan-Boltzmann constants, respectively. Once the initial configuration has been computed, the polytropic index of the non-relativistic gas is fixed at $\Gamma = 5/3$ during the simulations. We emphasize that the tori are initially not in perfect equilibrium.[1] This is due to the fact that the effective polytropic index of the gas and radiation mixture may not be exactly 4/3, and because in constructing the torus radiation field we have neglected the radiation pressure force along the radiative flux However, as long as we are interested in the time-varying behaviour of the tori, this should not be regarded as a weak point. Actually, in order to trigger the development of oscillations, all the models are perturbed by addition of a small radial velocity component, which is a rescaling of the spherical accretion solution by Michel (1972), i.e.

$$v^r = \eta\, v^r_{\rm Michel}\,. \qquad (2)$$

In practice, we act like in Zanotti et al. (2003), choosing a perturbation amplitude $\eta = 0.03$. A detailed study about the effects of different directions of the initial velocity perturbation has been presented by Mishra et al. (2015) for hydrodynamic slender tori.

2.2 Numerical approach

We solve the general relativistic radiation-hydrodynamics equations in a Schwarzschild metric using the KORAL code (Sądowski et al. 2013, 2014) which evolves the gas component, the radiation field, and the interaction between them in a conservative way using Godunov, finite-difference methods. The radiation is evolved adopting the M1 closure scheme (Levermore 1984).

The simulations assume axisymmetry and run in 2.5 dimensions, that is, allowing for non-zero azimuthal vector components. We assume a black hole mass of $10M_\odot$ and evolve the models for roughly $1.2s$, corresponding to ~ 165 orbital periods at the pressure maximum of the initial model. The numerical domain extends from $r_{\rm min} = 5$ to $r_{\rm max} = 14$ along the radial direction, and from $\theta = \pi/2 - 0.3$ to $\theta = \pi/2 + 0.3$ along the θ direction, and it is covered by a uniform (in radius and polar angle) grid composed of 448×448 grid-points. We note that the radial resolution is therefore $\Delta r = 0.02$. Standard outflow/no-inflow boundary conditions are adopted at all the boundaries[2].

For simplicity, in this work we adopt only the scattering opacity $\kappa_s = 0.34$ cm^2/g, and we account for the Comptonization using the "black-body" method (see Sadowski & Narayan 2015). Since we do not assume any external heating source, the tori are expected to cool down by emitting the radiation that supports them.

3 RESULTS

3.1 Torus dynamics

All the models have been evolved up to $t = 25000$, corresponding to ~ 165 orbital periods computed at the maximum density radius

[1] A truly equilibrium model for a thermodynamic torus around a black hole, which is however not valid for ideal gas equations of state, has been described in Zanotti (2014).

[2] Such a setup effectively prevents the torus from being self-illuminated, which could in principle affect (and complicate) its dynamical behaviour.

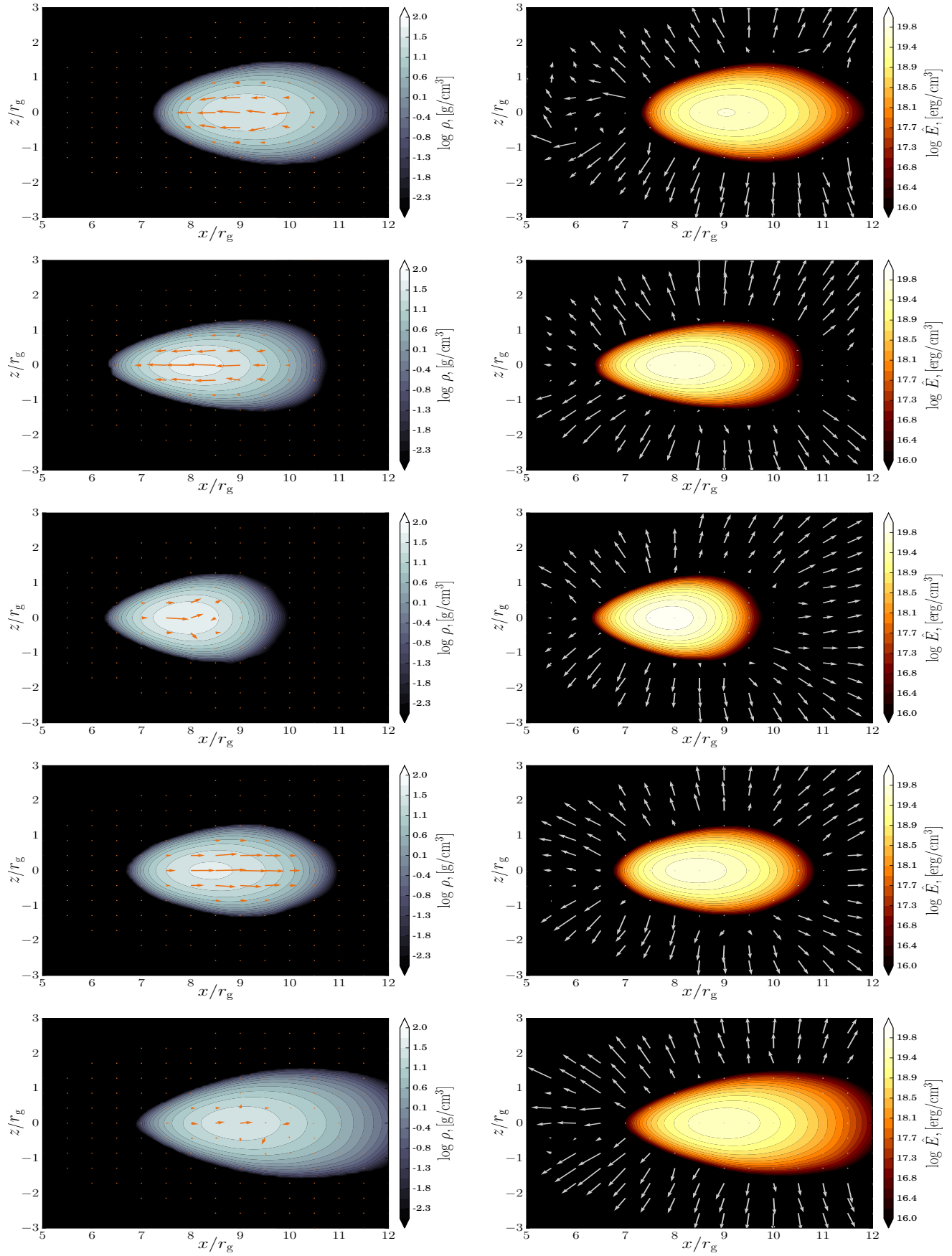

Figure 1. Illustration of a typical oscillation sequence for the model Rad30 through six snapshots (from top to bottom). Left panels: distribution of the rest-mass density with the velocity represented by orange arrows. Right panels: distribution of the energy density of the radiation field, with the energy flux represented by white arrows. For illustrative purposes, the $x-$ axis has been cut at 12.

© 0000 RAS, MNRAS **000**, 000–000

Name of the Model	$r_{\rm in}$	$r_{\rm out}$	$t_{\rm orb}$	Entropy	$T_{\rm c}$	$\rho_{\rm c}$	$\tau_{\rm sc}$
	[M]	[M]	[s]	[geo]	[K]	[g cm^{-3}]	
Hydro43	6.54	11.00	7.5×10^{-3}	100	4.82e9	1.63e8	n/a
Hydro53	-	-	-	100	9.65e9	1.59e8	n/a
Rad10	-	-	-	10	6.61e8	1.07e2	4.68e8
Rad30	-	-	-	30	2.95e8	3.88e1	1.73e7
Rad100	-	-	-	100	4.26e7	1.05e0	4.68e5
Rad400	-	-	-	400	4.23e7	1.64e-2	7.31e3

Table 1. Initial conditions of the considered tori. The mass of the black hole is assumed to be $M_{\rm BH} = 10 M_\odot$. The columns report: the inner and outer radii of the torus, the orbital period at the maximum density radius $r_c = 8.35$, the specific entropy (in $c = G = 1$ units), the temperature, the rest-mass density and the scattering opacity, the last three computed at r_c.

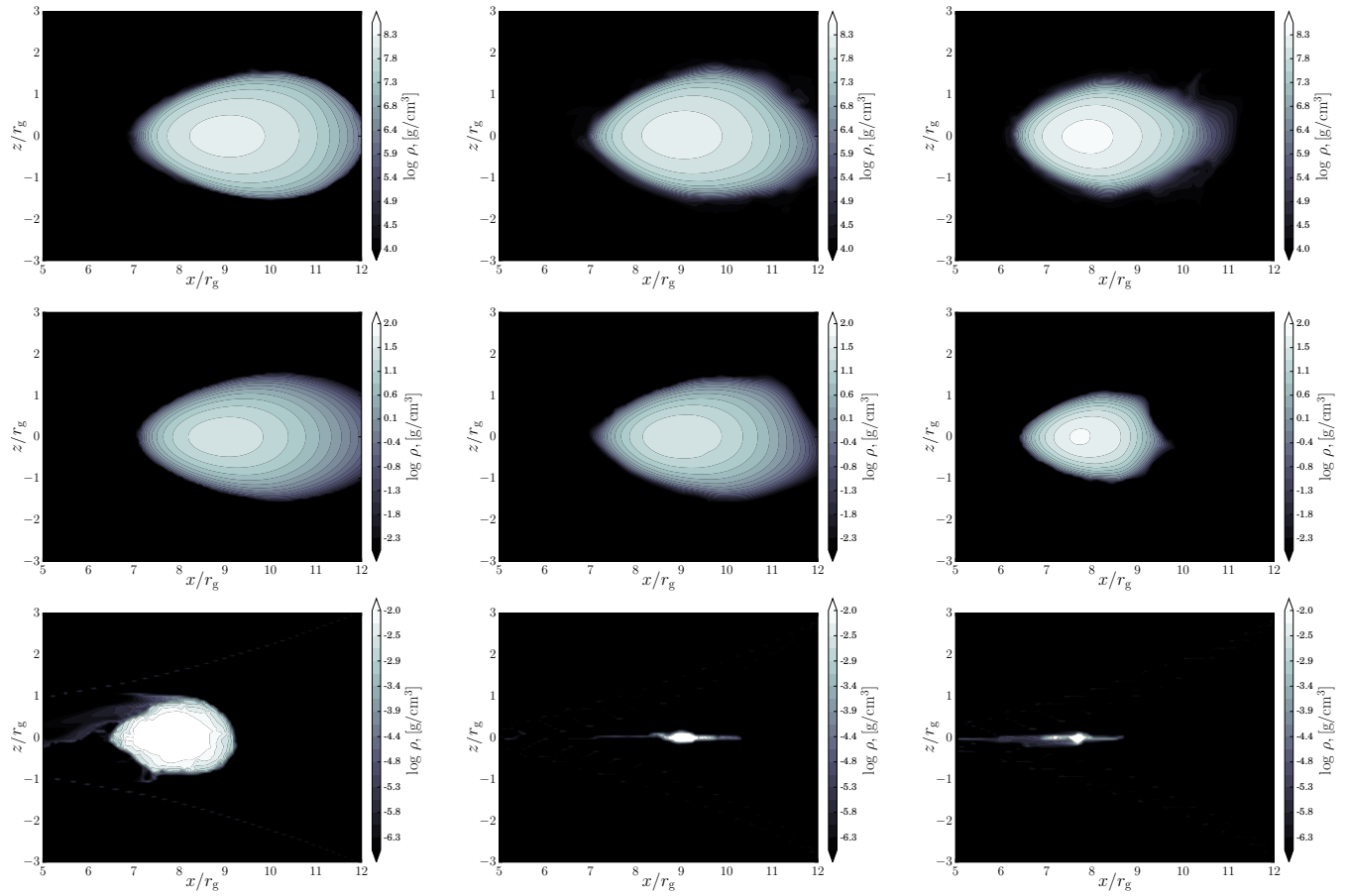

Figure 2. Rest-mass density distribution of the models Hydro53, Rad30 and Rad400, from top to bottom. First column: snapshot at $t \approx 1000 \approx 0.049$ s. Second column: snapshot at $t \approx 10000 \approx 0.49$ s. Last column: snapshot at the end of the simulation. The snapshots are chosen in such a way to represent the same phase of oscillation for each model. The density profile range covers 4.5 orders of magnitude. The density scale for the model Hydro53 is different from the other two.

$r_c = 8.35$. Two purely hydrodynamic models, namely Hydro43 and Hydro53, have been also studied, in order to provide a comparison with respect to the radiative models, which is especially useful in the spectral analysis of Sect. 3.2.

Because of the radial perturbation introduced, the tori start oscillating in the potential well. However, since the initial models are significantly below the marginally stable configuration, no appreciable mass accretion is induced by the oscillations and the periodic behaviour can last for a long time. In Fig. 1 a full oscillation sequence at $t \sim 0.1$ s is monitored through six snapshots for the model Rad30. The left and the right panels report the distribution of the rest-mass density and of the radiation energy density, respectively. The arrows in the radiative panels reflect the free-streaming radiation leaving the torus surface. As expected, during the evolution the energy density of the radiation remains concentrated towards the center of the torus, where the optical depth is the largest. Radiation diffuses out following the gradient of radiative energy density and ultimately leaves the surface of the torus. The distribution of the out coming radiation is determined by the shape of the photosphere. In the case of the tori studied here, most of the radiation is emitted roughly in the direction perpendicular to the equatorial plane.

Additional insight on the dynamics can be inferred from Fig. 2, whose rows compare the hydrodynamic model Hydro53 (top row), with the two radiation models Rad30 (middle row) and Rad400 (bottom row). We recall that at time $t = 0$ the three models

have the same size. The most dramatic behaviour is exhibited by the highest entropy and lowest optical depth model Rad400, which can be regarded as an extreme case. Initially, this model is the most radiation-pressure dominated but after 80 orbital periods it has lost most of its radiation, entering a phase of pure hydrodynamic evolution. Fig. 2 can indeed be interpreted in parallel with the information provided by Fig 3, where we have reported, for each of the radiative models, the evolution of the radiation-to-pressure ratio. The lower the specific entropy (see Table 1), the smaller is the initial value of $p_{\rm rad}/p_{\rm gas}$, but, simultaneously, the slower is the decay of $p_{\rm rad}/p_{\rm gas}$ during the evolution, since more photons are trapped in the more optically thick gas. As a result, while the models Rad10 and Rad30 preserve most of their radiation content for tens of orbital periods, the model Rad400, with a smaller optical thickness, quickly evaporates by radiation emission, collapsing towards a much smaller structure along the equatorial plane, as evident from the last row of Fig. 2.

The energy outcome from the oscillating tori is illustrated in Fig. 4, where we have reported the luminosity, in units of erg s^{-1}, and computed by means of a simple integral of the radiative fluxes through a suitable outer surface that encloses the whole oscillating torus. This quantity is a measure of radiation emitted by the torus, but it does not exactly correspond to the luminosity reaching an observer, for which the ray-tracing of photons would be needed (see Mishra et al. 2015, for such an approach in the purely hydrodynamic framework). There is a clear periodic pattern in the light curves that we obtain, which we will analyze more closely in the next Section. While collapsing towards the equatorial plane, the model Rad400 cools down quickly and loses the radiation that supported it, until it reaches a new quasi-stationary regime characterized by a luminosity one order of magnitude smaller than the initial value.

However, by far the most convenient quantity to highlight the periodic response of the torus to the external perturbation is the L_2-norm of the rest-mass density, computed as,

$$||\rho||_2 = \sum_{ij} \rho_{ij}^2 dV_{ij}\,, \tag{3}$$

where the summation extends all over the computational domain and ρ_{ij} and dV_{ij} are the density and the volume of cell ij, respectively. We have reported this quantity in Fig. 5. It is interesting to note that, at least qualitatively, the amplitude of the oscillation, as well as its frequency, do not seem to change appreciably among the different models, nor they seem to depend on whether there is a radiation field or not. However, these comments will become quantitative in the discussion of Sect. 3.2. The peculiar behaviour of the model Rad400 is represented in Fig. 6. As commented above, this model has a huge initial value of the ratio $p_{\rm rad}/p_{\rm gas}$, but it is also the least optically thick compared to the others, exhausting rapidly its radiation content. As a result of the drastic size reduction, the rest-mass density and the corresponding L_2-norm increase with time, until the torus enters a gas pressure dominated phase. This transition is well represented in Fig. 6, where the L_2-norm of the rest-mass density settles into an oscillating plateau after $t \sim 0.52$ s.

3.2 Spectral analysis

It is interesting to investigate the effects of radiation field on the spectra of oscillating tori. To this extent, we have performed a Fourier analysis of the L_2-norm of the rest mass density within the torus, which is reported in Fig. 7. Being a global quantity, the L_2-norm is particularly suitable for highlighting global modes of oscil-

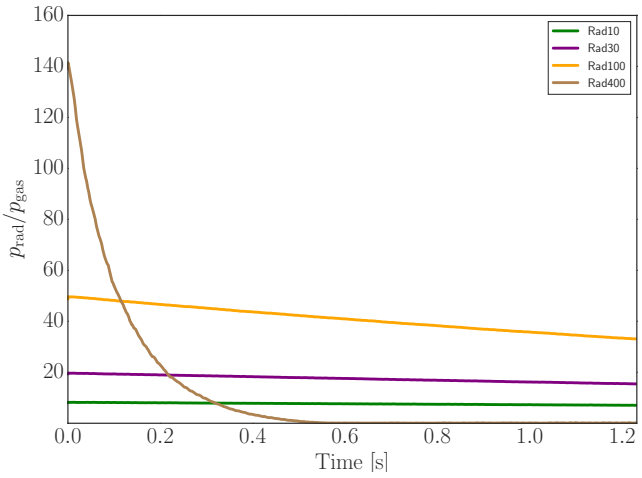

Figure 3. Radiation-to-gas pressure ratio as a function of time. Systems with the lowest entropy are preserving the ratio $p_{\rm rad}/p_{\rm gas}$ for the whole evolution. A drastic transition is observed for the model Rad400.

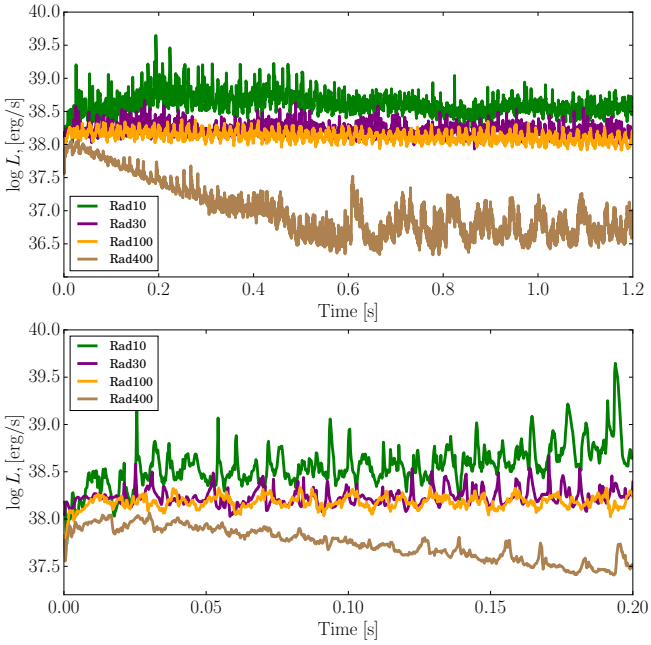

Figure 4. Top panel: Luminosity as a function of time for the full simulation period. Bottom panel: Zoom of the luminosity during the first 0.2 s.

lations. The first two spectra, marked in red and in blue, correspond to the purely hydrodynamic models, and, as usual, they serve us as a reference when comparing with the radiative models. In practice, two inertial-acoustic modes are detected, i.e. a fundamental mode f and an overtone o_1, with a ratio $f/o_1 \sim 1.47$. In addition to them, a sequence of linear combinations, such as 2f, $f + o_1$, $o_1 - f$, are also found, which is a well known coupling effect in physical systems governed by non-linear equations. All these results confirm what already found by Zanotti et al. (2003); Zanotti et al. (2005) and are also in very good agreement with linear perturbative analysis performed by Rezzolla et al. (2003). Although it is not our aim to extend the linear perturbative analysis to radiation-hydrodynamics tori in equilibrium, it is interesting to note that, for our specific

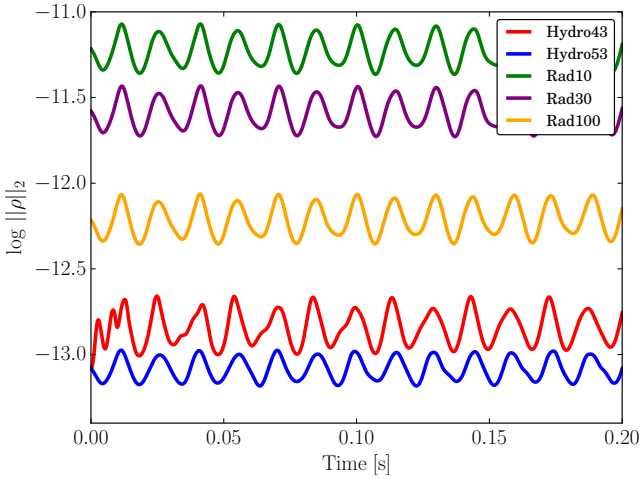

Figure 5. Evolution of the L_2 norm of the rest-mass density up to $t = 0.2$ s. The values for the radiative models had been rescaled to be visible in approximately the same range of the hydrodynamic models. See Fig 6 for the same quantity in the model Rad400.

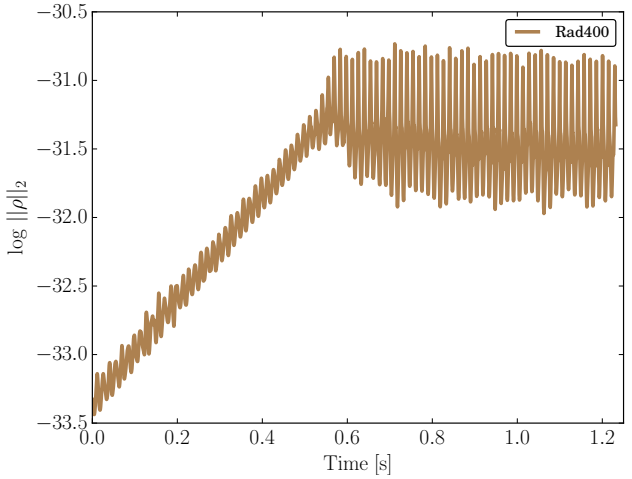

Figure 6. Evolution of the L_2 norm of the rest-mass density for the model Rad400.

hydrodynamics models with $\ell = 3.8$, the value of the ratio o_1/f predicted by the linear analysis of Rezzolla et al. (2003) is 1.47, which matches perfectly with that inferred from the red curve in Fig. 7. There is however a detail which was not noticed in the previous investigations, namely the fact that, while the fundamental mode f does not depend on the polytropic index Γ, the overtone o_1 does depend on it, slightly increasing with increasing Γ. This may indicate that in the mode o_1 the acoustic contribution is significant, while in the mode f the inertial contribution is dominant. We also recall that the frequency of the fundamental mode f tends to the epicyclic frequency at the radius of the maximum density in the limit of vanishing size tori (Rezzolla et al. 2003). In our models the epicyclic frequency at $r_c = 8.35$ (the maximum density radius) is $f_{\rm epic} \sim 71$ Hz, while the fundamental model f in Fig. 7 is at 68 Hz.[3] Hence, the major contribution to f comes from the epicyclic term, and the dependence on Γ is essentially lost. We also note that the f and o_1 modes found here may correspond to the so called *radial* and *plus* modes of slender tori, according to the terminology introduced by Blaes et al. (2006).[4]

When migrating to the radiative models, the spectra maintain a good qualitative agreement with the purely hydrodynamic ones. In particular, all the modes f, o_1 and 2f are still clearly visible. Apart from the model Rad400, which becomes gas-pressure dominated after $t \sim 0.5$ s, all the others are radiation-pressure dominated all over the evolution. Consistently with that, their mode o_1, which is sensible to the value of Γ, approaches the value obtained by the Hydro43 model with $\Gamma = 4/3$.

Moreover, in the spectra of Rad10, Rad30 and Rad100 there are good indications for the presence of a genuinely new mode of oscillation, marked as r_1 for the model Rad10 at approximately $r_1 \sim 6.39 \times 10^{-3} M_{\rm BH}^{-1} \sim 129.8 M_{\rm BH}^{-1}$ Hz and totally absent in the spectra of Hydro43 and Hydro53. Our claim that the mode r_1 is due to the radiation field could be rigorously confirmed after performing a linear perturbative analysis of the relativistic radiation-hydrodynamics equations, which is however far beyond the scope of the present work. The spectrum of the model Rad400 is much more noisy than the others and in practice only the fundamental mode f is clearly visible. This is true both in the radiation-pressure phase of the evolution, with a corresponding spectrum marked as Rad400-rad in Fig. 7, and in the gas-pressure phase, with a corresponding spectrum marked as Rad400-gas. This is not surprising, given that the dynamics of this model is so violent, causing the torus to collapse to a much thinner disc and no longer able to work as a cavity for the inertial-acoustic modes.

For comparison, in Fig. 8 we have reported also the spectra of the luminosity (Fig. 4), pertinent to the radiative models. Although these spectra reproduce the same kind of pattern described above, they are significantly more noisy than those of Fig. 7. In particular, the identification of the mode r_1 is much more dubious. From one side, this is understandable, since the luminosity is a highly non-linear derived quantity. From another side, this is disappointing, since this is the quantity that would be more prone to potential observations, but from which we could not extract the richer information that is contained in Fig. 7. Our results should also be compared with those of Schnittman & Rezzolla (2006), who computed the light curves from oscillating tori by using a ray-tracing code. In their case the power spectra of the light curves are equivalent to those obtained from the spectra of purely dynamic quantities. As we have shown, however, when the back reaction of radiation onto matter is properly taken into account through a time dependent radiation-hydrodynamic code, the imprint of the dynamics into the observable quantities is less transparent.

4 CONCLUSIONS

In this work we have studied the radiation-hydrodynamics evolution of relativistic tori that are subject to external perturbations. To this extent, we have performed high resolution two dimensional general relativistic simulations in the Schwarzschild metric with the KORAL code, which can successfully capture both the optically thick and the optically thin regime through the relativistic version of the M1-closure. The evolution is followed for $\sim$ 165 orbital periods. Depending on the optical thickness of the initial config-

[3] These numbers apply for our specific torus model and assuming $M_{\rm BH} = 10 M_\odot$.

[4] See also the discussion in Mishra et al. (2015).

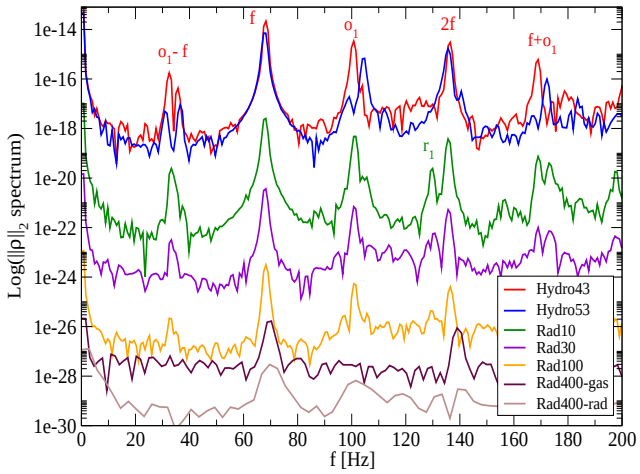

Figure 7. Spectrum of the L_2 norm of the rest-mass density. The fundamental mode, the overtones and their linear combinations are marked for the Hydro43 model (red curve). The units of the vertical axis are arbitrary.

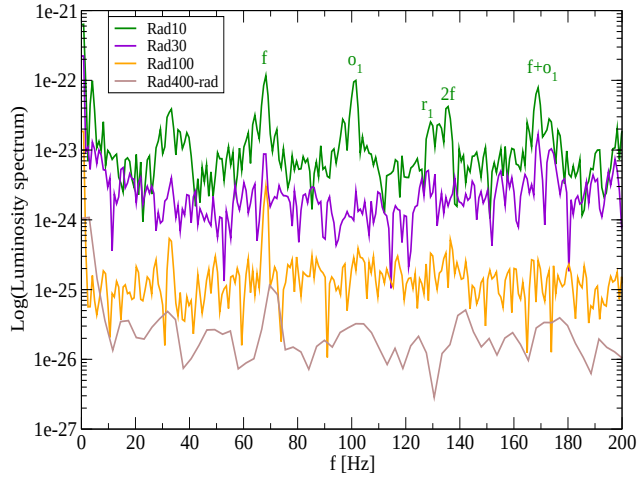

Figure 8. Spectrum of the luminosity. The units of the vertical axis are arbitrary.

uration, the torus can either remain radiation pressure dominated, or migrate towards the gas pressure dominated regime, after experiencing a rapid dynamical collapse. The periodic response induced by the external perturbation manifests in all the thermodynamics quantities, and in particular in the emitted luminosity, which in the most optically thick models can reach values as high as $L \sim 10^{38} - 10^{39}$ erg s^{-1}.

In addition to the standard inertial-acoustic oscillations already highlighted by Zanotti et al. (2005) for purely hydrodynamic models, we have found a new mode in the spectra of the L_2-norm of the rest-mass density, with a clear peak at a frequency $129 M_{\rm BH}^{-1}$ Hz. This mode, which is absent in the purely hydrodynamic evolution, can be attributed to the radiation with a high degree of fidelity. These results suggest that the interpretation of kHz-QPOs in the X-ray spectra of Low Mass X-ray binaries in terms of inertial-acoustic oscillations (Rezzolla et al. 2003) must necessarily be extended to take into account the role of a radiation field.

Finally, the power spectra obtained from the light curves are substantially more noisy than those extracted from the dynamic quantities, which should sound as a caveat for those cases in which the interaction of radiation and matter is not properly taken into account.

5 ACKNOWLEDGEMENTS

G.P.M. acknowledges support by Polish NCN grant 2013/09/B/ST9/00060. O.Z. acknowledges support by the European Research Council (ERC) under the European Union's Seventh Framework Programme (FP7/2007-2013), ERC Grant agreement no. 278267. A.S. acknowledges support by NASA through Einstein Postdoctoral Fellowship PF4-150126 awarded by the Chandra X-ray Center, which is operated by the Smithsonian Astrophysical Observatory for NASA under contract NAS8-03060.

We would also like to acknowledge PRACE for awarding access to the SuperMUC supercomputer based in Munich, Germany at the Leibniz Rechenzentrum (LRZ).

REFERENCES

Abramowicz M., Jaroszynski M., Sikora M., 1978, Astron. Astrophys., 63, 221
Abramowicz M. A., Fragile P. C., 2013, Living Reviews in Relativity, 16
Abramowicz M. A., Karas V., Kluzniak W., Lee W. H., Rebusco P., 2003, Pub. Astron. Soc. Japan, 55, 467
Bakala P., Goluchová K., Török G., Šrámková E., Abramowicz M. A., Vincent F. H., Mazur G. P., 2015, Astron. Astrophys., 581, A35
Blaes O. M., Arras P., Fragile P. C., 2006, Mon. Not. R. Astron. Soc., 369, 1235
Blaes O. M., Šrámková E., Abramowicz M. A., Kluźniak W., Torkelsson U., 2007, Astrophys. J., 665, 642
Farris B. D., Li T. K., Liu Y. T., Shapiro S. L., 2008, Phys. Rev. D, 78, 024023
Fishbone L. G., Moncrief V., 1976, Astrophys. J., 207, 962
Font J. A., Daigne F., 2002, Mon. Not. R. Astron. Soc., 334, 383
Fragile P. C., Gillespie A., Monahan T., Rodriguez M., Anninos P., 2012, ArXiv e-prints
Kozlowski M., Jaroszynski M., Abramowicz M. A., 1978, Astron. and Astrophys., 63, 209
Levermore C. D., 1984, Journal of Quantitative Spectroscopy and Radiative Transfer, 31, 149
Mazur G. P., Vincent F. H., Johansson M., Šramková E., Török G., Bakala P., Abramowicz M. A., 2013, Astron. Astrophys., 554, A57
McKinney J. C., Tchekhovskoy A., Sadowski A., Narayan R., 2013, ArXiv e-prints
Michel F. C., 1972, Astrophys. Spa. Sci., 15, 153
Mishra B., Vincent F. H., Manousakis A., Fragile P. C., Paumard T., Kluźniak W., 2015, ArXiv e-prints
Montero P. J., Zanotti O., 2012, Mon. Not. R. Astron. Soc., 419, 1507

Novikov I. D., Thorne K. S., 1973, in Black Holes (Les Astres Occlus) Astrophysics of black holes.. pp 343–450
Remillard R. A., McClintock J. E., 2006, Ann. Rev. Astron. Astroph., 44, 49
Rezzolla L., Yoshida S., Maccarone T. J., Zanotti O., 2003, Mon. Not. R. Astron. Soc., 344, L37
Rezzolla L., Yoshida S., Zanotti O., 2003, Mon. Not. R. Astron. Soc., 344, 978
Roedig C., Zanotti O., Alic D., 2012, Mon. Not. R. Astron. Soc., 426, 1613
Sadowski A., Narayan R., 2015, ArXiv e-prints
Sądowski A., Narayan R., McKinney J. C., Tchekhovskoy A., 2014, Monthly Notices of the Royal Astronomical Society, 439, 503
Sądowski A., Narayan R., Tchekhovskoy A., Zhu Y., 2013, Mon. Not. R. Astron. Soc., 429, 3533
Schnittman J. D., Rezzolla L., 2006, Astrophys. J., 637, L113
Shakura N. I., Sunyaev R. A., 1973, Astron. Astrophys., 24, 337
Takahashi H. R., Ohsuga K., 2013, Astrophys. J., 772, 127
Vincent F. H., Mazur G. P., Straub O., Abramowicz M. A., Kluźniak W., Török G., Bakala P., 2014, Astron. Astrophys., 563, A109
Zanotti O., 2014, Astronomy and Astrophysics, 563, A17
Zanotti O., Font J. A., Rezzolla L., Montero P. J., 2005, Mon. Not. R. Astron. Soc., 356, 1371
Zanotti O., Rezzolla L., Font J. A., 2003, Mon. Not. Roy. Soc., 341, 832
Zanotti O., Roedig C., Rezzolla L., Del Zanna L., 2011, Mon. Not. R. Astron. Soc., 417, 2899